

Supplementary Information for
**Insights into Electrochemiluminescence Dynamics by Synchronizing
Real-Time Electrical, Luminescent, and Mass Spectrometric
Measurements**

Xuemeng Zhang,^a Weifeng Lu,^a Cheng Ma,^{a, c} Tao Wang,^a Jun-Jie Zhu,^a Richard N. Zare,^b and Qianhao Min^{*a}

^a. State Key Laboratory of Analytical Chemistry for Life Science, Chemistry and Biomedicine Innovation Center, School of Chemistry and Chemical Engineering, Nanjing University, Nanjing 210023, P. R. China

^b. Department of Chemistry, Stanford University, Stanford, California 94305, USA

^c. School of Chemistry and Chemical Engineering, Yangzhou University, Yangzhou 225002, China

***Corresponding authors**

E-mail: minqianhao@nju.edu.cn (Qianhao Min)

Table of Content

- S-3 – S-7 Experimental Section
- S-8 Configuration and parameters of the RT-Triplex setup
- S-9 Attribution analysis of the potential-dependent increase of MS signals
- S-10 Effect of flow rate on identification of short-lived intermediates
- S-11 Real-time EC-MS analysis of electrooxidation reaction of DMA
- S-12 Cyclic voltammogram of flunitrazepam in bulk solution
- S-13 Proposed mechanism for electrochemical dimerization of luminol
- S-14 Localization of the luminol luminescence in the three-electrode system
- S-15 Negative-ion-mode mass spectrum of luminol at pH 11
- S-16 – S-18 Identification of the ion at m/z 162.0195 in luminol ECL system by MS/MS
- S-19 – S-21 Identification of L·OOH-H₂O, L·OH, L·OOH, and luminol dimer by MS/MS
- S-22 Electrochemical dimerization of luminol in acidic condition
- S-23 – S-24 Identification of luminol dimer and oxidized luminol dimer by MS/MS
- S-25 The effect of O₂ on ECL intensity at pH 7 and 11
- S-26 – S-28 Electrochemical impedance spectroscopy (EIS) of the RT-Triplex
- S-29 Zoomed-in mass spectra of BODIPY^{•+} and by-products
- S-30 Structural identification of the dehydrogenated by-products in the BODIPY system
- S-31 MS monitoring of dimerized BODIPY **B2** during electrooxidation
- S-32 MS/MS spectra of BODIPY^{•+} and by-products
- S-33 – S-34 The effect of increasing TPrA on electrogenerated species of BODIPY **B1** and **B2**
- S-35 – S-36 Verification of the “catalytic route” in the BODIPY/TPrA ECL system
- S-37 Cyclic voltammograms of TPrA and BODIPY **B1**
- S-38 Cyclic voltammograms of DMA, flunitrazepam, luminol and BODIPY in given conditions
- S-39 – S-44 Detailed information on intermediates and products in this work
- S-45 References

Experimental section

1. Chemicals and reagents

Flunitrazepam, *N,N*-dimethylaniline (DMA), luminol, lithium triflate (LiOTf). and formic acid were purchased from Sigma-Aldrich (St. Louis, MO, USA). Acetic acid and ammonium acetate were obtained from Shanghai Reagent Co. (Shanghai, China). 1,3,5,7,8-Pentamethyl-2,6-diethyl-4,4-difluoro-3*a*-azonia-4*a*-aza-4-bora(V)-*s*-indacene-4-ide (BODIPY **B1**), 4,4-difluoro-1,3,5,7,8-pentamethyl-4-bora-3*a*,4*a*-diazas-indacene (BODIPY **B2**), and 4,4-difluoro-8-phenyl-3*a*-azonia-4*a*-aza-4-bora(V)-*s*-indacene-4-ide (BODIPY **B3**) were purchased from J&K Scientific Ltd. (Beijing, China). Tri-*n*-propylamine (TPrA), 3-aminophthalic acid (AP), and ammonium hydroxide were purchased from Aladdin Reagent Co., Ltd (Shanghai, China). Polydimethylsiloxane (PDMS) was purchased from Dow Corning, Midland, MI. Acetonitrile (ACN) and methanol (MeOH) were of chromatographic grade from Merck (Darmstadt, Germany). Ultrapure water was obtained from MilliQ gradient ultrapure water system (Millipore Inc., MA, USA). All other chemicals were of analytical grade without further treatment.

2. Fabrication of capillary EC microreactor

As shown in Figure S1, the capillary EC microreactor consists of a PDMS reservoir (volume 600 μ L), a fused-silica capillary (I.D. 200 μ m, O.D. 360 μ m, length 11 cm) and a three-electrode system with a platinum wire (Φ 100 μ m) going through the capillary as working electrode (WE), another platinum wire (Φ 500 μ m) as counter electrode (CE), and a silver wire as quasi-reference electrode (QRE) (Φ 500 μ m) (Figure S1a). In detail, the mold for PDMS reservoir was fabricated in a petri dish (I.D. 3.5 cm). First, one sink and four access holes were reserved by fixing a 2.5 mL centrifuge tube (O.D. 1 cm) upside-down in the center of the petri dish and inserting four syringe needles (O.D. 500 μ m) from side to center (1 mm from the bottom). Then the PDMS prepolymer mixture (mass ratio of monomer and curing agent = 10:1) was poured into the petri dish mold and cured horizontally at 70 $^{\circ}$ C for 5 h. After pulling out the centrifuge tube together with the four syringe needles, the annular block of

PDMS was peeled from the dish and pasted onto the plain glass slide (5.5 cm × 5.5 cm) to create the PDMS reservoir.

To minimize the diffusion of species generated on WE, a narrow reaction space was created by inserting a Pt wire WE (Φ 100 μm , length 16 cm) into a fused-silica capillary (I.D. 200 μm , O.D. 360 μm , length 11 cm). Then the fused-silica capillary with Pt wire WE inside was inserted into PDMS reactant reservoir, and WE was led out through another access hole to connect with the electrochemical workstation (Figure S1a and S1b). In addition, the polyimide coating of the capillary part inside the reservoir was burned off to ensure that the ECL emission on the WE was detected by a PMT placed below. The distance between the reservoir wall and capillary end was shortened to 1 mm (Figure S1c). Finally, the Pt wire CE and the Ag wire QRE were inserted into the PDMS reservoir through the remaining two access holes and connected to the electrochemical workstation.

3. Construction of Venturi easy ambient sonic-spray ionization source

To avoid extra in-source EC reactions, V-EASI with no need for high voltage was used to generate sonic spray in RT-Triplex. In detail, the capillary EC microreactor, as inner capillary and emitter passed through a Swagelok tee tube and an outer capillary (I.D. 530 μm , O.D. 700 μm , length 1 cm), and extended 1 mm beyond the outer capillary (Figure S1 b and S1d). Meanwhile, the distance between the emitter capillary and the MS inlet was optimized to be 2 mm for stable ion signal and flow rate. A high-velocity N_2 stream flowed through the outer capillary, generating Venturi self-pumping effect to ensure a stable and continuous spray. The flow rate of solvent was optimized by adjusting the N_2 pressure (Figure S3a). This design allows reactant solution from the PDMS reservoir to be rapidly transferred into and then mobilized out of the capillary EC microreactor after redox reaction at the central Pt wire WE, in which all the electrogenerated species can be monitored by MS.

4. Electrochemical methods

Electrochemical measurements were carried out on a CHI instrument electrochemical workstation (CHI760E, CH Instruments Inc.). Cyclic voltammograms

of DMA were obtained in the capillary EC microreactor at a scan rate of 10 mV/s ranging from 0 V to 1.5 V in ACN containing 1 mM LiOTf. Cyclic voltammograms of 25 μ M flunitrazepam were obtained at a scan rate of 20 mV/s ranging from 0 V to -1.5 V in MeOH/H₂O (1:1, v/v) containing 1% formic acid. The potential step experiments were done using chronoamperometry (CA) by applying alternately 0 V and 1.5 V on the WE.

Electrochemical impedance spectroscopy (EIS) measurement was performed on a Metrohm Autolab electrochemical workstation (PGSTAT 302, Eco Chemie., Switzerland) with a three-electrode system. The amplitude of the applied sine wave potential was 10 mV, and the frequency range was from 100000 Hz to 0.01 Hz.

5. Electrochemiluminescence methods

The ECL data were acquired using a model MPI-E electrochemiluminescence analyzer (Xi'an Remax Analytical Instrument Co. Ltd., Xi'an, China). The ECL reaction of luminol was performed by potential linear scan from 0 to 1.5 V at a scan rate of 10 mV/s in 1 mM luminol in ACN/H₂O (1:1, v/v) containing 10 mM ammonium acetate, in which the pH was finely adjusted by addition of ammonium hydroxide or acetic acid. The ECL measurements of BODIPY systems were performed by potential linear scan from 0 to 1.5 V at a scan rate of 20 mV/s to record the anodic ECL. Acetonitrile containing 1 mM LiOTf was used as the electrolyte in the ECL analysis of BODIPY. All ECL signals were collected with a PMT operated with a working voltage at 900 V and a triple amplification series.

6. Mass spectrometry

All MS data were acquired on an LTQ Orbitrap XL hybrid mass spectrometer (Thermo Fisher Scientific, San Jose, CA, USA). The Orbitrap ion transfer capillary was held at 285°C, and the resolution was set to 30,000 for all analyses. All data were analyzed using the Qual Browser feature of the Xcalibur™ program (Thermo Fisher Scientific, San Jose, CA).

In the three-channel synchronous acquisition experiment, the mass spectrometer kept on scanning when the EC/ECL methods were initiated to run. The moment of triggering

the EC/ECL programs was defined as time zero, after which the applied potential, measured current, luminescence strength, and mass spectrum were synchronously and continuously acquired in real time.

The tandem mass (MS/MS) spectra of intermediates from luminol ECL reaction were obtained on negative ion mode by using collision induced dissociation (CID) energy of 20 eV. In BODIPY system, the ion collision energy was adjusted 30 eV to obtain abundant MS/MS fragmented ions of intermediates on positive ion mode.

7. Modified RT-Triplex setup

To separate electrochemical reaction at electrode interfaces from the following homogeneous reaction in bulk solution, the RT-Triplex setup was further modified. As shown in Figure 6b, an auxiliary fused-silica capillary (I.D. 200 μm , O.D. 360 μm , length 10 cm) was inserted into the reservoir with the terminal nearby the inlet of the capillary EC microreactor. In this manner, the TPrA solution could be freely injected through this auxiliary capillary into the reaction system at any time.

Typically, we designed the experiment to assess the possibility of homogeneous reaction between TPrA and newly formed BODIPY^{•+} at the EEI. First, the WE potential was fixed at 1.5 V for 0.5 min, while the reactant solution (BODIPY or blank solution) passed through the capillary EC microreactor and generated stable spray via VESI. After the moment when the potential was switched from 1.5 V to 0 V, 10 μL 1 mM co-reactant TPrA solution was promptly infused into the PDMS reservoir through the auxiliary capillary with a syringe. The electrical, luminescence and mass spectrometric signals were collected by the RT-Triplex platform throughout the process.

Configuration and parameters of the RT-Triplex setup

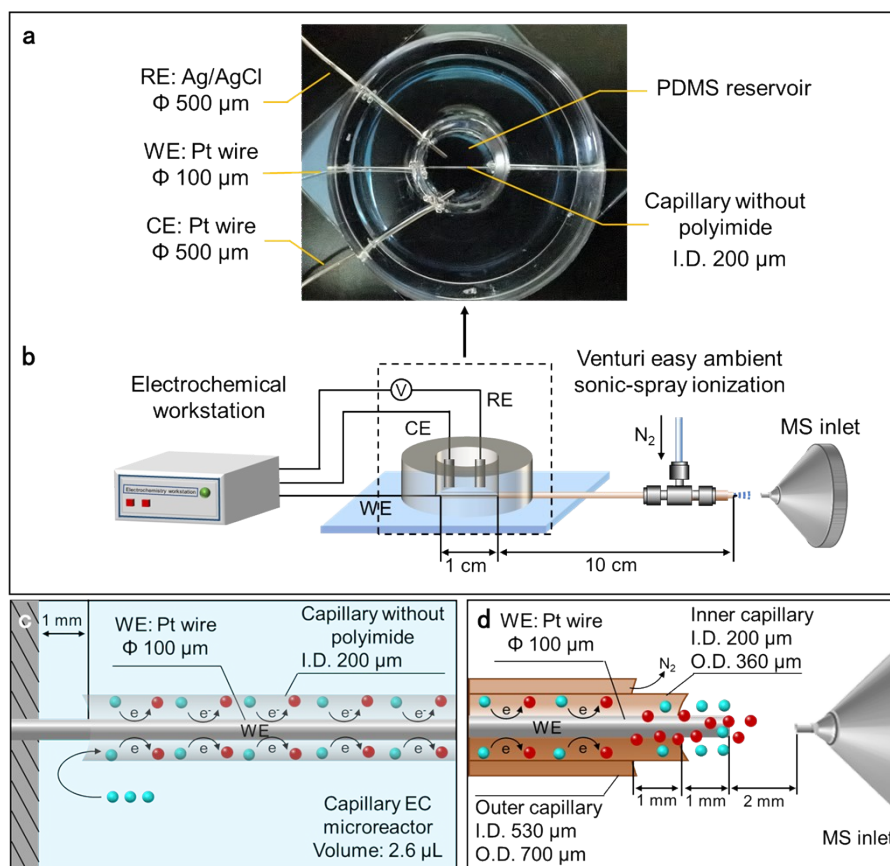


Figure S1. (a) Photograph showing the parameters of PDMS reservoir and capillary EC microreactor. (b) Schematic illustration of the established RT-Triplex platform. (c, d) Schematics showing the configuration and parameters of the two ends of capillary EC microreactor.

Attribution analysis of the potential-dependent increase of MS signals

To verify that the potential-dependent elevation of MS intensity originated from occurrence of electrochemical reactions, the electrooxidation of redox inactive phenylboronic acid (PBA) was performed in ACN/H₂O (1:1, v/v) containing 1 mM LiOTf at a Pt wire WE. As compared with blank solution, no obvious oxidation peak was observed in the cyclic voltammogram (CV) of PBA from 0 V to 2 V at a scan rate of 100 mV/s (Figure S2a). Accordingly, ion signal of protonated PBA exhibited no increase in the extracted ion chromatography (EIC) upon applying the voltage. This control experiment further verified that the increase of ion signals (e.g., DMA⁺, TMB⁺, and [TMB+H]⁺) in the EC system along with the applied voltage was indeed originating from ongoing EC reactions.

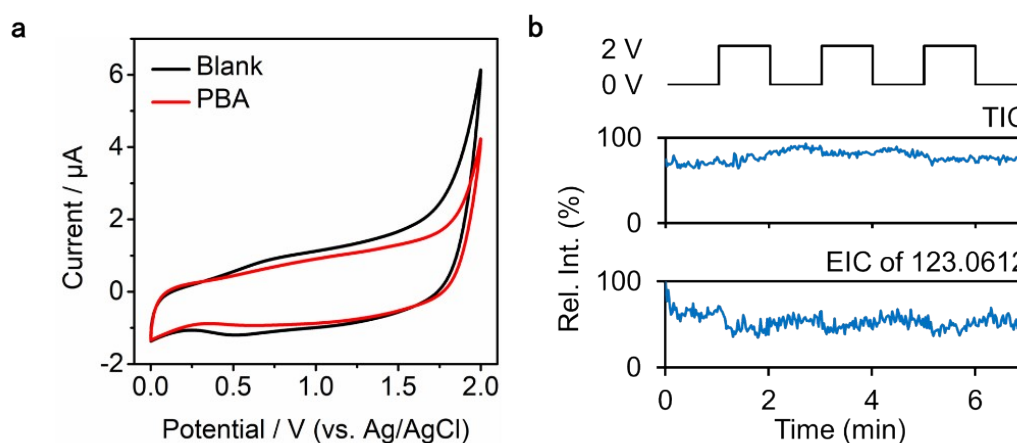


Figure S2. (a) Cyclic voltammograms of blank solution (ACN/H₂O (1:1, v/v) containing 1 mM LiOTf and 1 mM PBA at a scan rate of 0.1 V/s at a Pt wire WE. (b) The TIC and EIC of m/z 123.0612 (protonated PBA) during potential switching between 0 V and 2 V.

Effect of flow rate on identification of short-lived intermediates

The flow rate of solvent was controlled by the sheath N₂ pressure. As shown in Figure S3a, the flow rate increased with the sheath N₂ pressure for all the three types of solvent. When the pressure was raised to 0.55 MPa, the flow rate of ACN, ACN/H₂O (1:1, v/v), and MeOH/H₂O (1:1, v/v) reached 152 μL/min (linear velocity 0.108 m/s), 68 μL/min (linear velocity 0.0483 m/s), and 46 μL/min (linear velocity 0.0327 m/s), respectively. In addition, the rapid mobility of newly created species facilitated the identification of the fleeting intermediate from EEI by MS. As shown in Figure S3b, when the N₂ pressure rise to 0.45 MPa, the ion signal of DMA⁺ (*m/z* 121.0886) was detected while applying 1.5 V oxidation potential to WE.

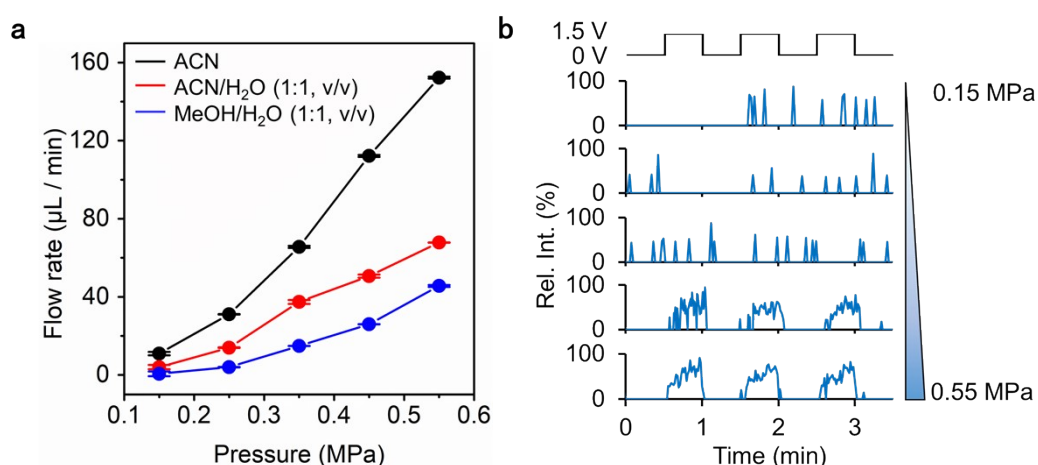


Figure S3. (a) The relationship between sheath N₂ pressure and flow rate of different solvents. (b) Voltage-dependent EICs of *m/z* 121.0886 (DMA⁺) varied with different N₂ pressure (0.15 MPa, 0.25 MPa, 0.35 MPa, 0.45 MPa, and 0.55 MPa).

Real-time EC-MS analysis of electrooxidation reaction of DMA

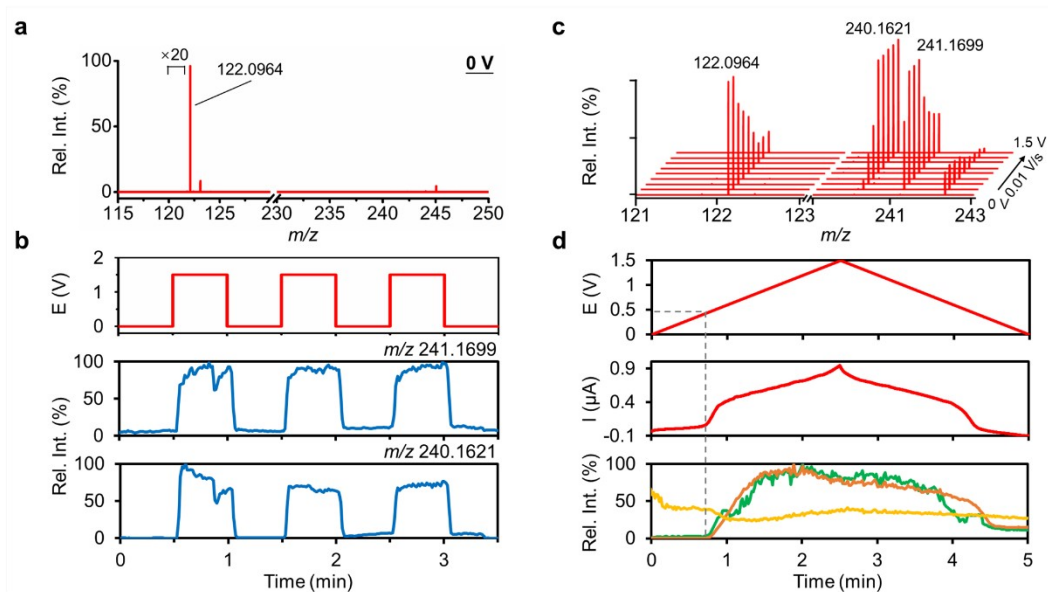


Figure S4. (a) Positive-ion-mode mass spectrum of 94 μM DMA in acetonitrile (ACN) containing 1 mM lithium triflate without potential applied to the Pt wire WE. (b) The EICs of m/z 241.1699 and 240.1621 as a function of the applied potential. (c) Positive-ion-mode mass spectra of the above DMA system obtained at different voltage points during the potential sweep. (d) The applied potential, measured current, and EICs of m/z 122.0964 (yellow), 241.1696 (green), and 240.1618 (orange) during the time in which the potential was linearly scanned from 0 V to 1.5 V at a scan rate of 10 mV/s in ACN containing 94 μM DMA and 1 mM LiOTf.

Cyclic voltammogram of flunitrazepam in bulk solution

The electrochemical response of 25 μM flunitrazepam was characterized by cyclic voltammetry from 0 V to -1.5 V at a scan rate of 20 mV/s in the bulk solution of MeOH/H₂O (1:1, v/v) containing 1% formic acid with a glassy carbon WE. On the negative-going scan, two reduction peaks centered at -0.46 V and -0.79 V vs Ag/AgCl were observed. As previously reported, the first peak was the result of the four-electron, four-proton ($4e^-$, $4H^+$) reduction of the nitro group to hydroxylamine (R1 and R2), and the second peak corresponds to the two-electron, two-proton ($2e^-$, $2H^+$) reduction of azomethine group (R4).^{1,2} However, the reactions R3 and R5 cannot be found in the CV, and the peak voltages of R1 and R2 are too close to be clearly differentiated due to the limited potential resolution.

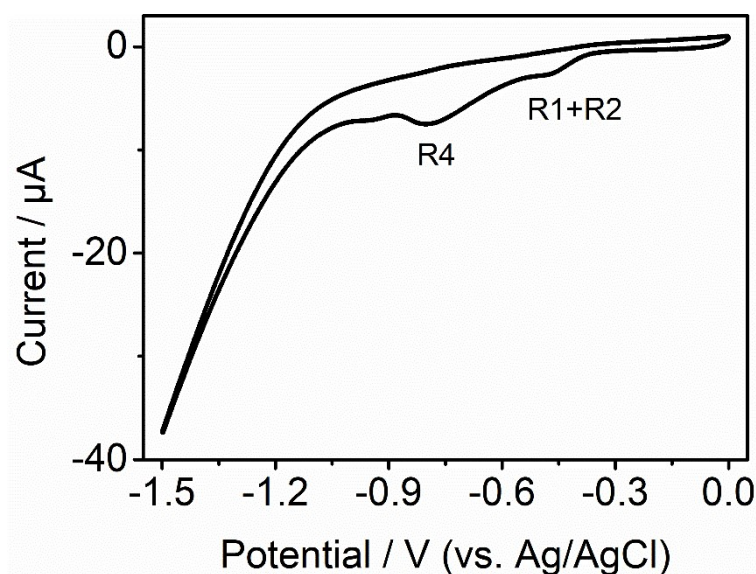


Figure S5. (a) Cyclic voltammogram of 25 μM flunitrazepam on a glassy carbon WE in the bulk solution of MeOH/H₂O (1:1, v/v) containing 1% formic acid from 0 V to -1.5 V at a scan rate of 20 mV/s.

Proposed mechanism for electrochemical dimerization of luminol

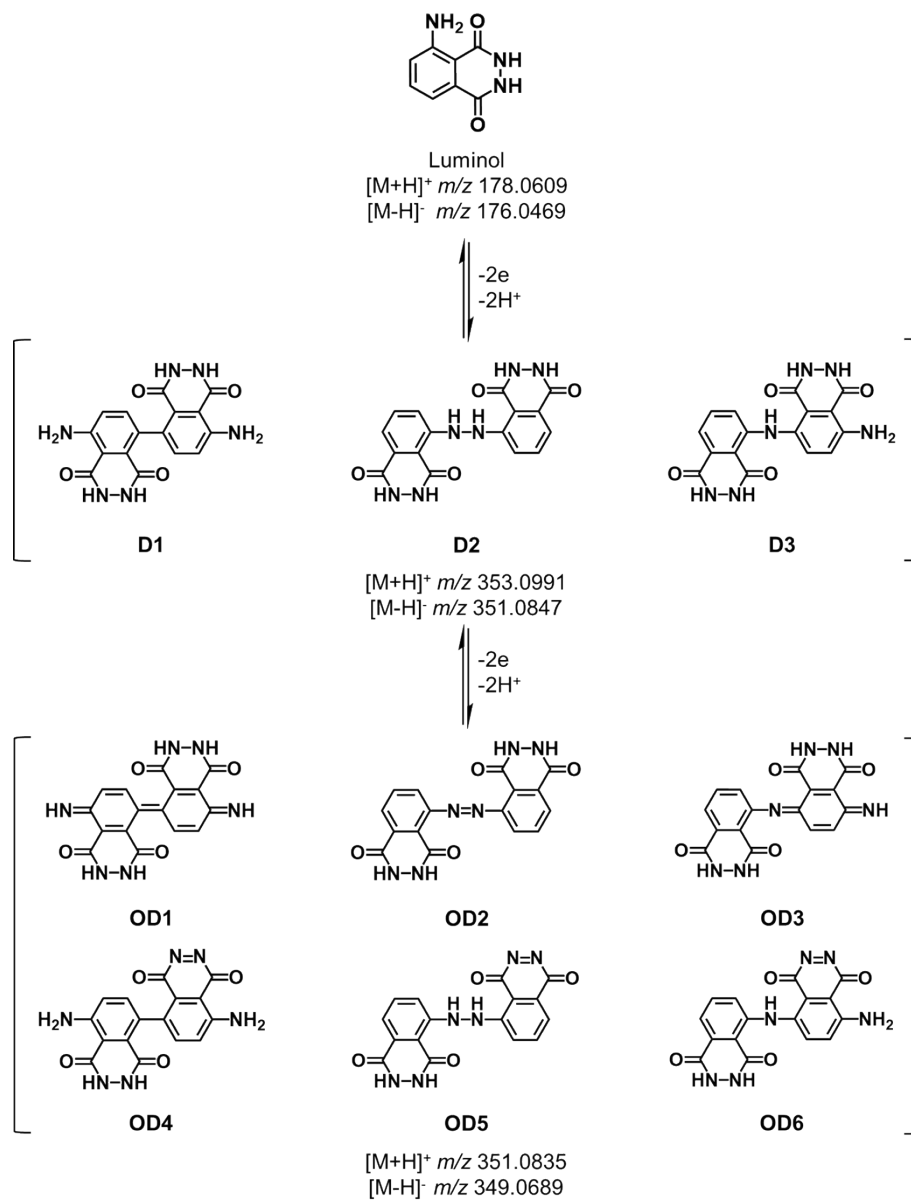


Figure S6. Proposed mechanism for electrochemical dimerization of luminol.^{3,4} The dimer and oxidized dimer are illustrated as several possible isomers which cannot be distinguished by MS.

Localization of the luminol luminescence in the three-electrode system

In the three-electrode system, the actual location of luminol ECL was determined by tuning the exposure areas of WE and CE. As shown in Figure S7a, the polyimide coating of the capillary part inside the reservoir was burned off to make the anode ECL detectable, leading to significant luminescence signal when applying oxidation potential (Figure S7d). In contrast, keeping the polyimide coating intact resulted in luminescence sharply declined by three orders of magnitude (Figure S7e), no matter if the Pt wire CE was extended or shortened (Figure S7b and c). This striking difference indicated that the Pt wire WE (anode in oxidation) was the actual location where luminol ECL occurs, while the contribution of probable cathode luminescence of luminol on CE could be neglected in our case.

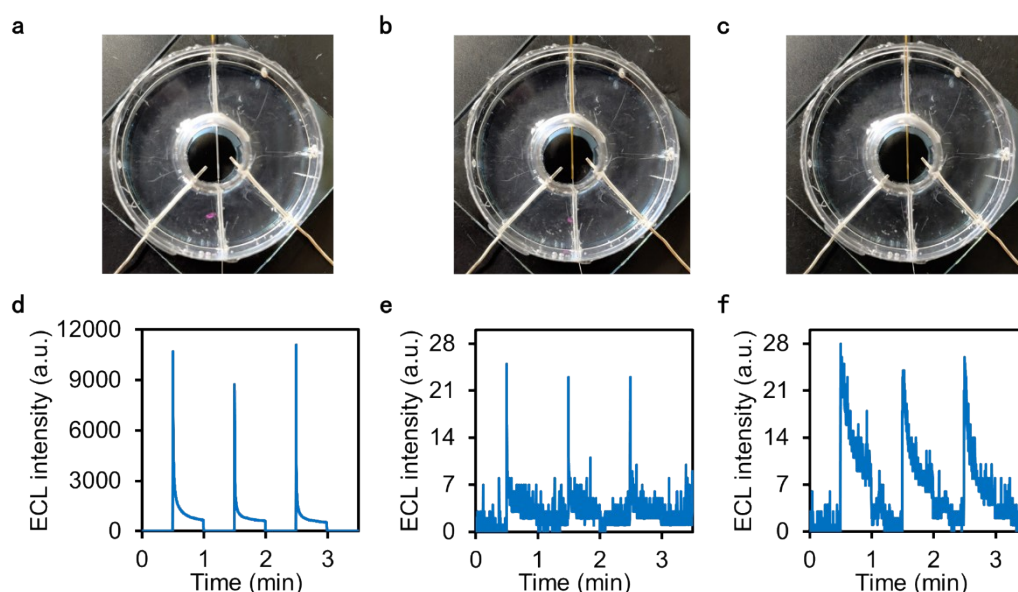


Figure S7. (a-c) Photographs of the three-electrode system equipped with a (b) transparent or (b) coated capillary EC microreactor, or (c) a shortened Pt wire CE. (d-e) The corresponding ECL-time curves along with the oxidation potential switched between 0 V and 1.5 V.

Negative-ion-mode mass spectrum of luminol at pH 11

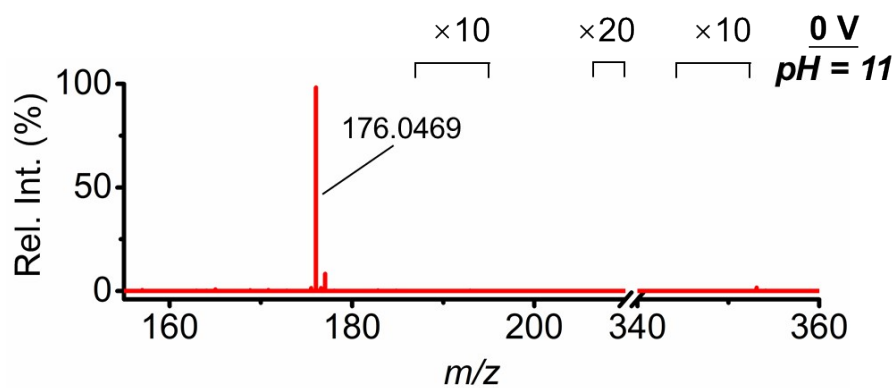


Figure S8. Negative-ion-mode mass spectrum of 1 mM luminol in pH 11 ACN/H₂O (1:1, v/v) containing 10 mM ammonium acetate with no applied potential.

Identification of the ion at m/z 162.0195 in luminol ECL system by MS/MS

To substantiate the ion signal at m/z 162.0195 was derived from the product 3-aminophthalic acid (AP), we employed the standard reagent to obtain the mass spectrum. The standard sample of AP (1 mM) in ACN/H₂O (1:1, v/v) containing 10 mM ammonium acetate at pH 11 was directly measured by the established RT-Triplex method without potential applied. As shown in Figure S9a, in addition to the deprotonated AP ([AP-H]⁻) at m/z 180.0299, a peak at m/z 162.0195 attributed to dehydrated AP (AP-H₂O) was observed. Upon CID, [AP-H]⁻ continuously lost two CO₂ molecules from carboxyl groups to generate daughter ions at m/z 136.0401 and 92.0503 (Figure S9b and S9c). As shown in Figure S9d and S9e, AP-H₂O was fragmented into daughter ions at m/z 118.0297 and 90.0348, supposed to be produced by neutral loss of CO₂ and CO.

Meanwhile, the ion at m/z 162.0195 generated in the luminol ECL system was subjected to CID fragmentation. As shown in Figure S10, tandem mass spectrum of m/z 162.0195 showed a daughter ion at m/z 118.0298 by losing one molecule of CO₂. Based on the identical accurate mass and similar MS/MS spectral patterns, we deduce that the ion m/z 162.0195 in the products of luminol ECL system was derived from dehydrated AP.

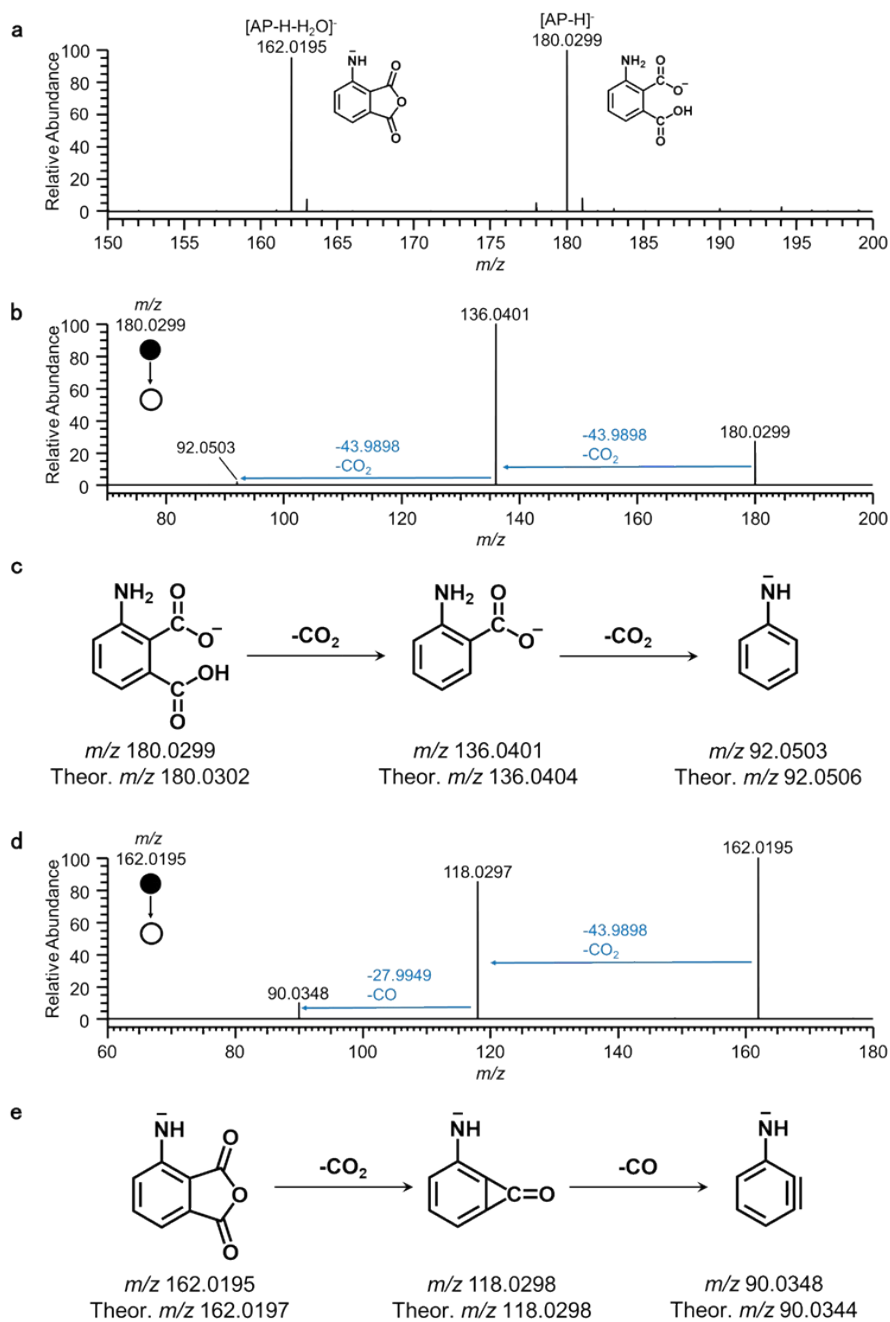


Figure S9. (a) Negative-ion-mode mass spectrum of 1 mM AP in ACN/H₂O (1:1, v/v) containing 10 mM ammonium acetate. Negative-ion-mode MS/MS spectra of (b) [AP-H]⁻ (m/z 180.0299) and (d) [AP-H-H₂O]⁻ (m/z 162.0195). Proposed CID fragmentation pathways of [AP-H]⁻ and [AP-H-H₂O]⁻ are shown in (c) and (e).

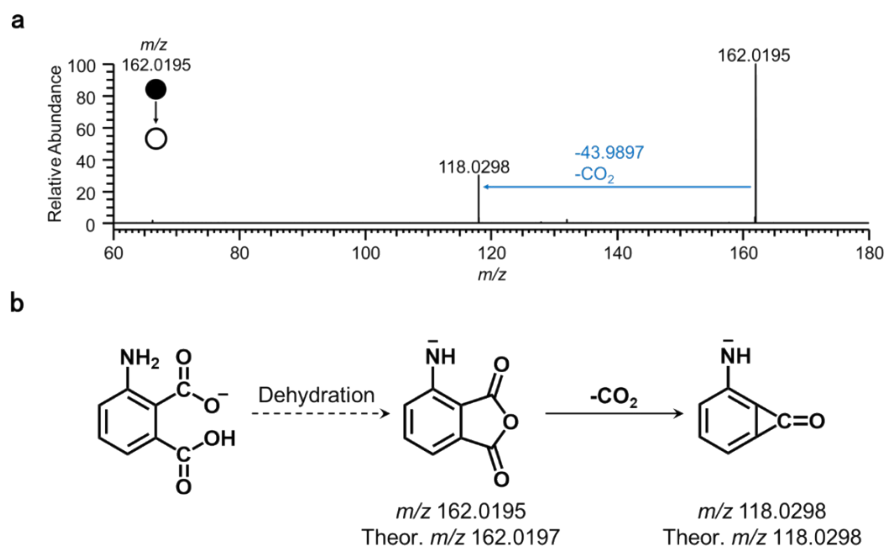


Figure S10. (a) Negative-ion-mode MS/MS spectrum of AP-H₂O (m/z 162.0195). (b) Proposed CID fragmentation pathway of AP-H₂O.

Identification of L-OOH-H₂O, L-OH, L-OOH, and luminol dimer by MS/MS

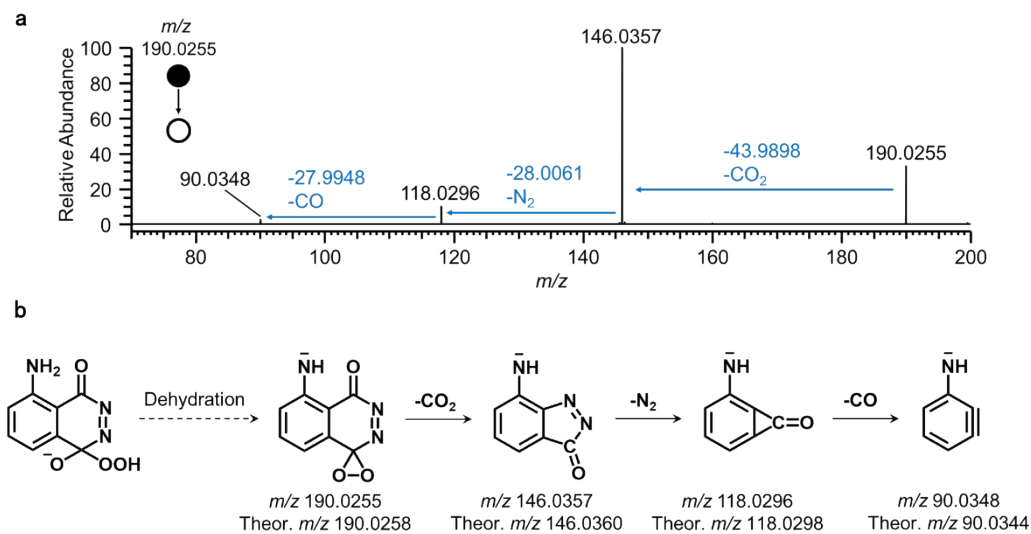


Figure S11. (a) Negative-ion-mode MS/MS spectrum of L-OOH-H₂O (*m/z* 190.0255). (b) Proposed CID fragmentation pathway of L-OOH-H₂O.

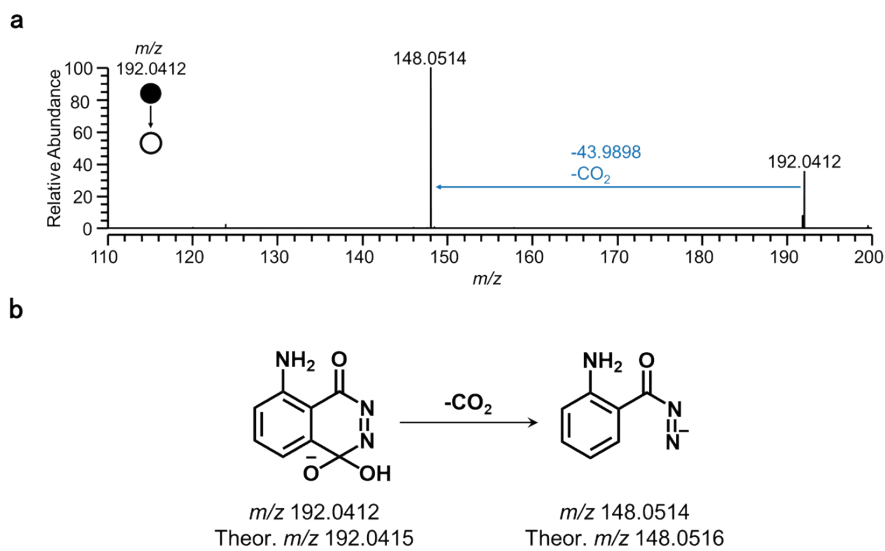
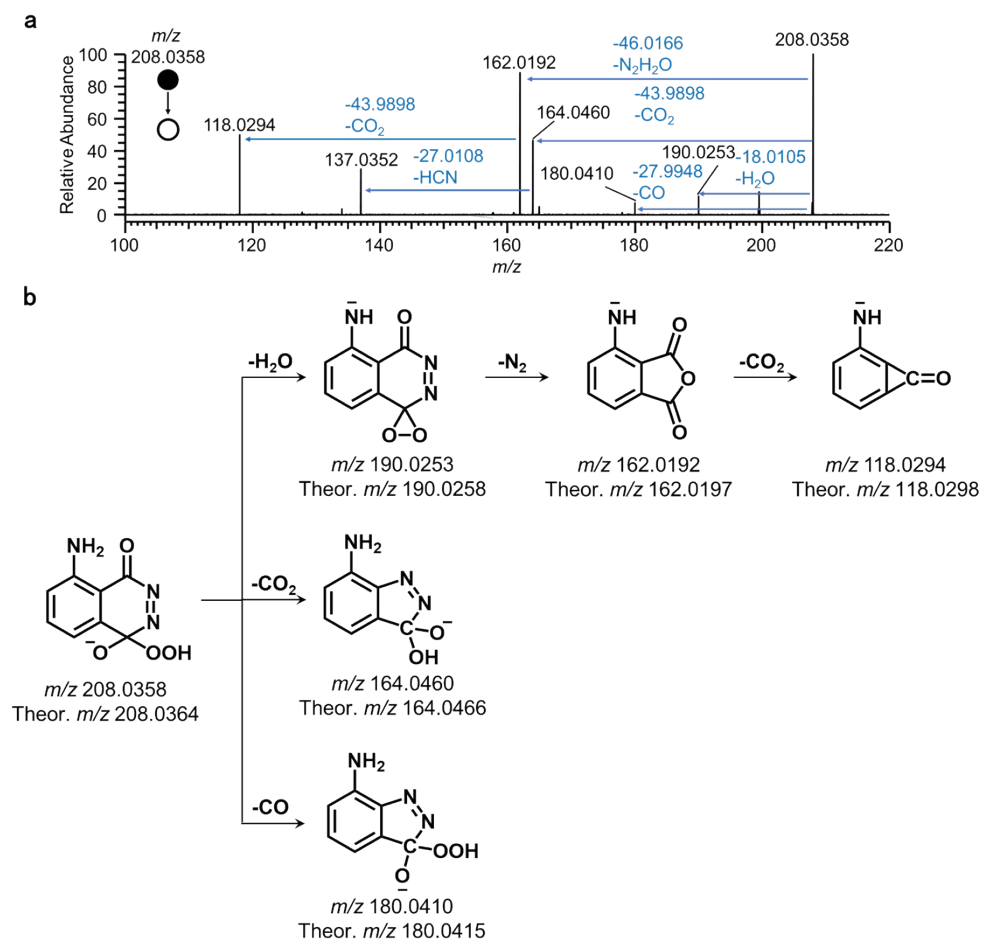


Figure S12. (a) Negative-ion-mode MS/MS spectrum of L-OH (*m/z* 192.0412). (b) Proposed CID fragmentation pathway of L-OH.



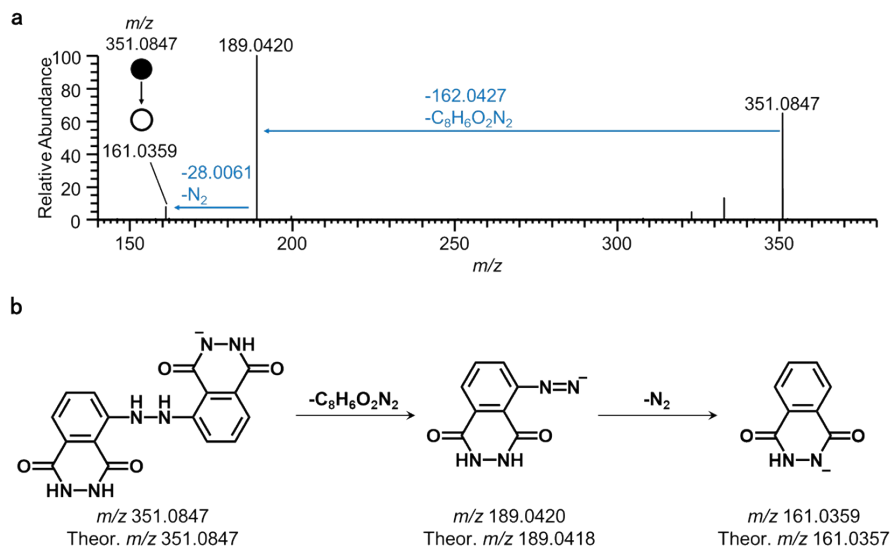


Figure S14. (a) Negative-ion-mode MS/MS spectrum of the luminol dimer (m/z 351.0847). (b) Proposed CID fragmentation pathway of the luminol dimer.

Electrochemical dimerization of luminol in acidic condition

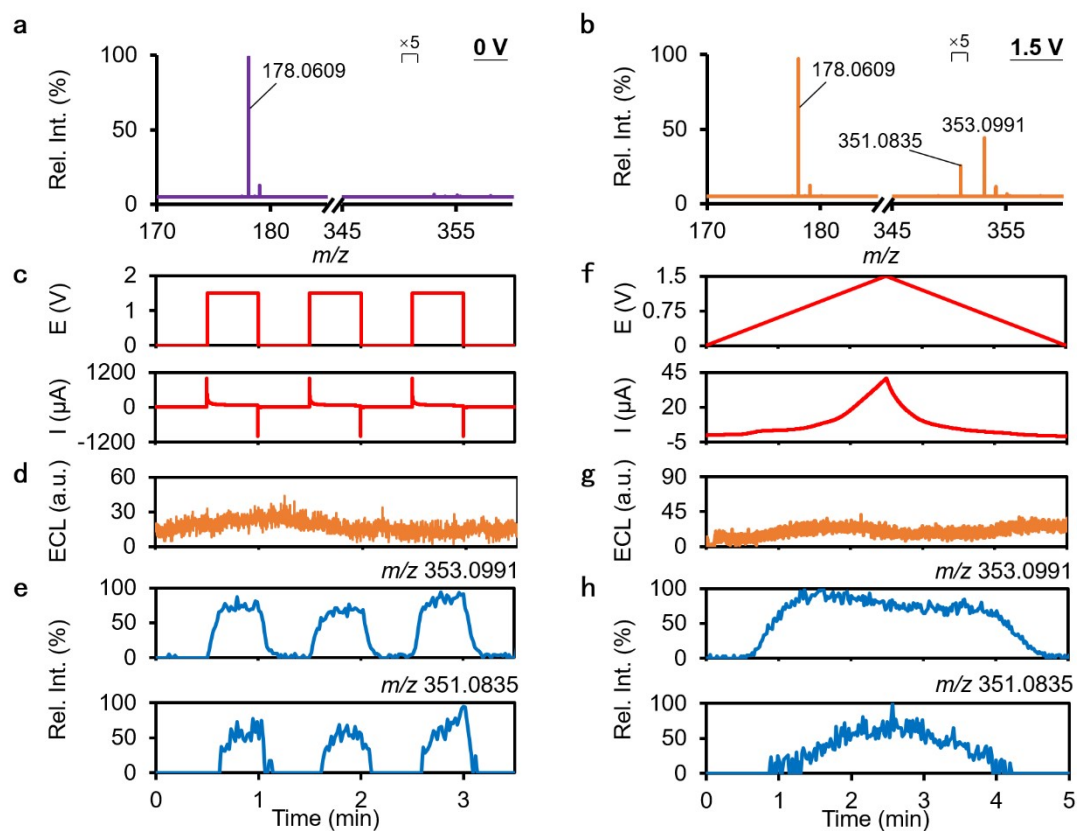


Figure S15. Positive-ion-mode mass spectra of 1 mM luminol with (a) 0 V and (b) 1.5 V applied to the Pt wire WE at pH 3. (c, f) The applied potential, measured current (d, g) ECL-time curve and (e, h) EICs of the dimer and oxidized dimer in the (c-e) potential step and (f-h) potential sweep experiments. Potential pulses were given at 1.5 V with a duration of 30 s and an interval of 30 s, and the CV scanning was performed between 0 V and 1.5 V at a scan rate of 10 mV/s.

Identification of luminol dimer and oxidized luminol dimer by MS/MS

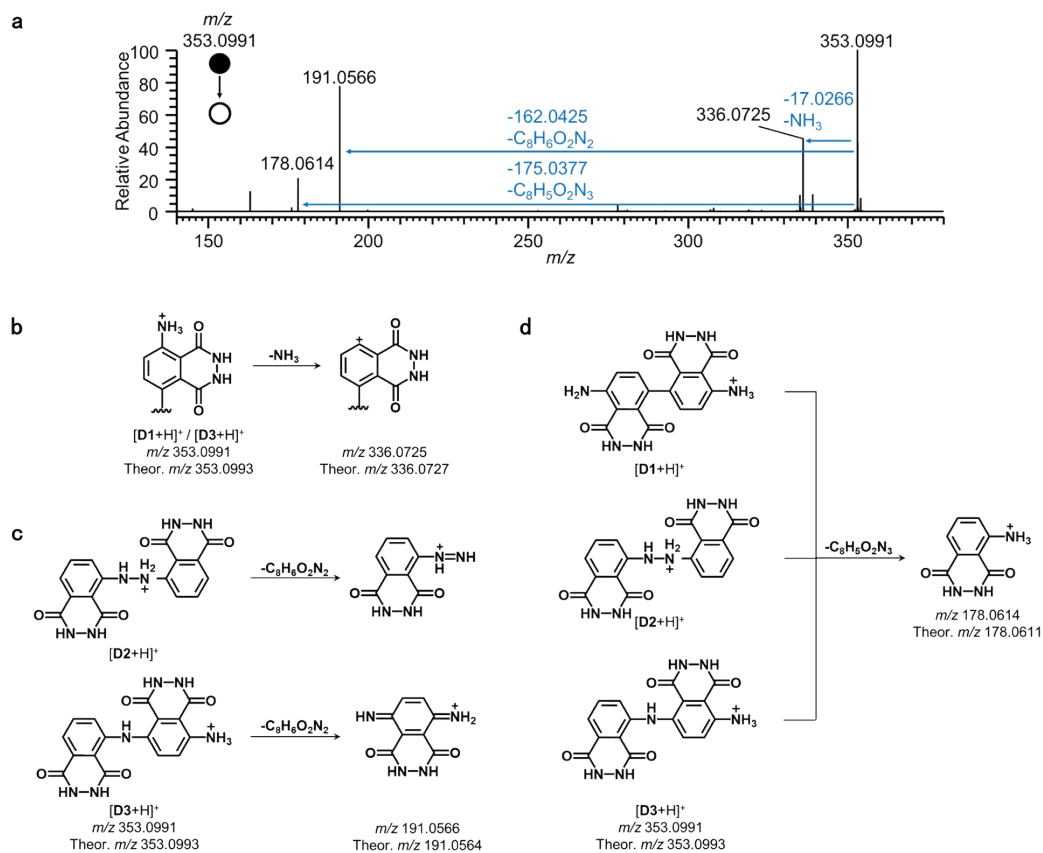


Figure S16. (a) Positive-ion-mode MS/MS spectrum of the luminol dimer (m/z 353.0991) obtained from electrooxidation of luminol at pH 7. (b-d) Proposed CID fragmentation pathways of the luminol dimer.

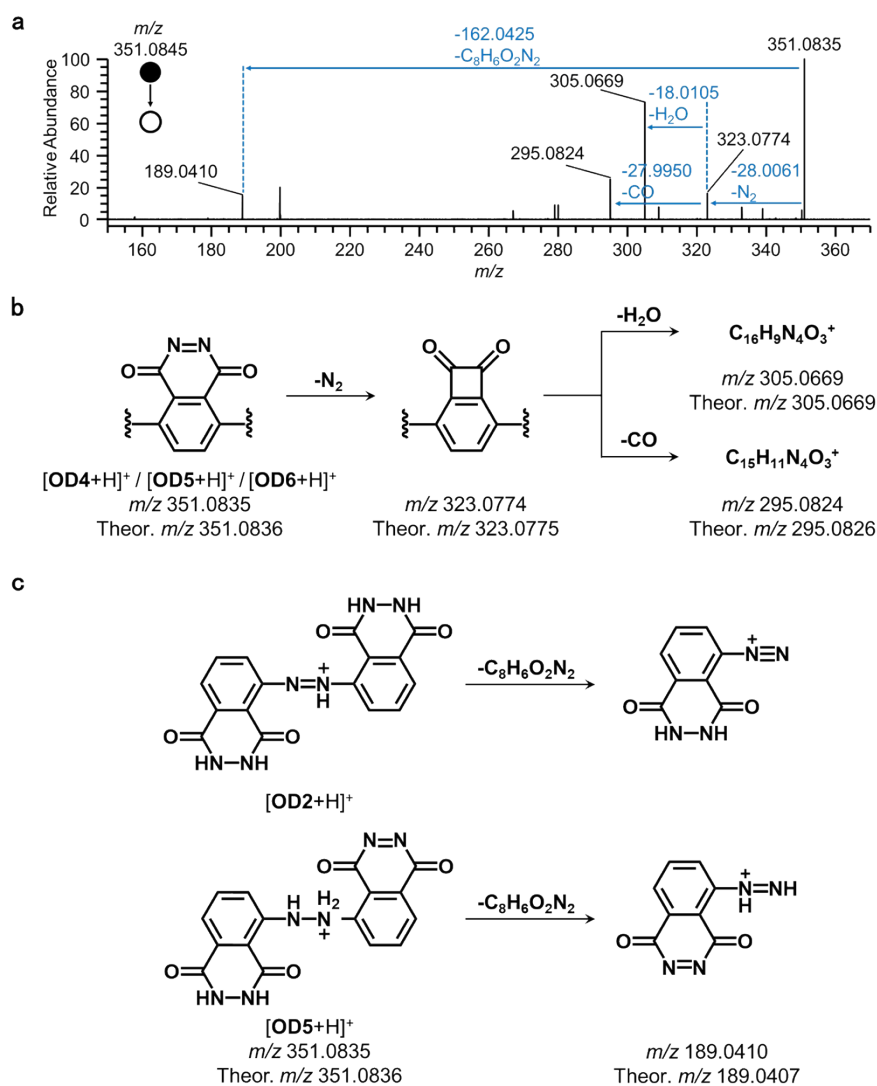


Figure S17. (a) Positive-ion-mode MS/MS spectrum of the oxidized dimer (m/z 351.0835) obtained from electrooxidation of luminol at pH 7. (b, c) Proposed CID fragmentation pathways of the oxidized luminol dimer.

The effect of O₂ on ECL intensity at pH 7 and 11

To clarify the influence of dissolved O₂ to anodic ECL of luminol, the ECL of luminol was measured by CV in normoxia and deoxygenated solution respectively under air and nitrogen atmosphere at pH 7 and 11. The dissolved oxygen was removed by bubbling nitrogen gas into the luminol solution. As shown in Figure S18a and S18b, no matter whether the solution was deoxygenated or not, the luminol ECL exhibited ignorable intensity at pH 7. In the alkaline medium, both the normoxia and deoxygenated luminol systems shared the similar ECL-voltage curve pattern. Of note, the strong ECL emission in the voltage range of 0.3-1.0 V was not weakened by the removal of oxygen (Figure S18c and S18d), indicating that dissolved oxygen makes little contribution to the luminol ECL in this voltage window.

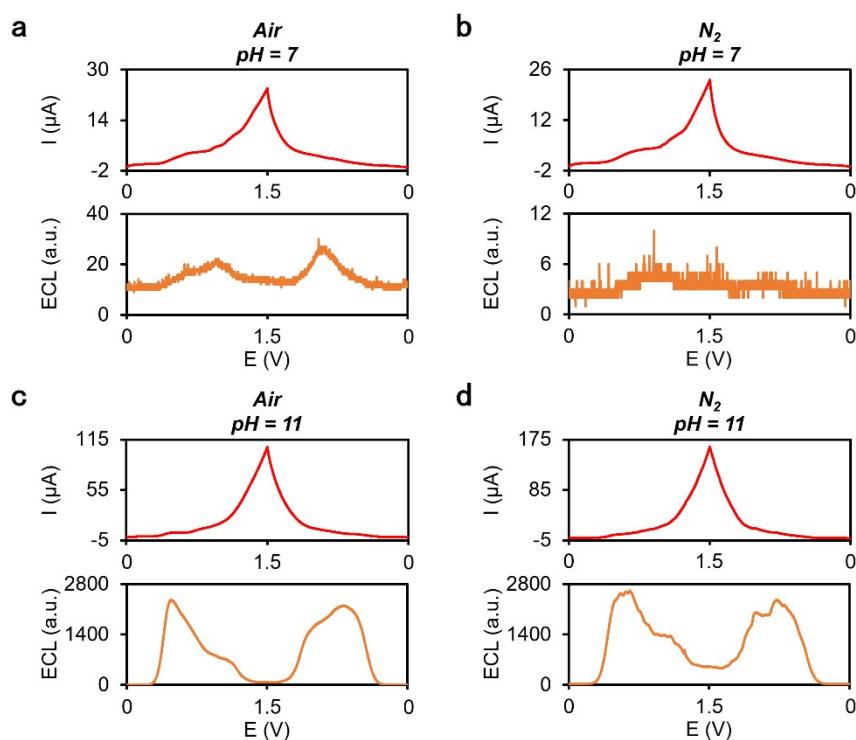


Figure S18. The measured current and ECL intensity of 1 mM luminol in capillary EC microreactor under (a, c) air and (b, d) nitrogen atmosphere at (a, b) pH 7 and (c, d) 11 during the CV scanning from 0 V to 1.5 V at a scan rate of 10 mV/s. All potentials were referred to the Ag wire QRE.

Electrochemical impedance spectroscopy (EIS) of the RT-Triplex

Electrochemical impedance spectroscopy (EIS) characterization of the RT-Triplex was presented with a three-electrode system in the ACN/H₂O (1:1, v/v) including 10 mM ammonium acetate and 1 mM K₃[Fe(CN)₆]/K₄[Fe(CN)₆] (solvent similar to the ECL system of luminol). As shown in Figure S2a-S2d, along with the reduction of Pt wire WE area in the capillary, the downward trend in the solution resistance (R_{Ω}) was observed, indicating that the excessively extended Pt wire WE in the capillary distant from RE contributed to the increase of R_{Ω} . In contrast, no obvious change of charge transfer resistance (R_{ct}) was observed in this experiment, due to the unchanged surface properties of the WE. To further investigate the influence of diffusion hindrance on the impedance, the capillary cover was thoroughly removed to expose Pt wire WE in the PDMS reservoir (Figure S2e). R_{Ω} and R_{ct} obtained from Nyquist plot were both significantly decreased, indicating that the capillary cover around Pt wire WE exerts negative influence on diffusion.

Our primary goal is to timely capture newly generated species at electrodes by MS when interfacial electrochemical reaction occurs. Considering the theme of our work, the extension of WE and capillary in a close proximity to MS inlet is physically necessary. Moreover, the aim of designing a capillary cover on the part of WE in the PDMS reservoir is to ensure the newly born species at WE being fully mobilized into gas phase instead of diffusing into bulk solution, which potentially degraded the detection instantaneity. Conclusively, the extended Pt wire WE and capillary cover in PDMS reservoir are all necessary in mass spectrometric and luminescence measurements, and the additional impedance contributed by this unique design elicited little impact on real-time capture and identification of electrochemically generated intermediates.

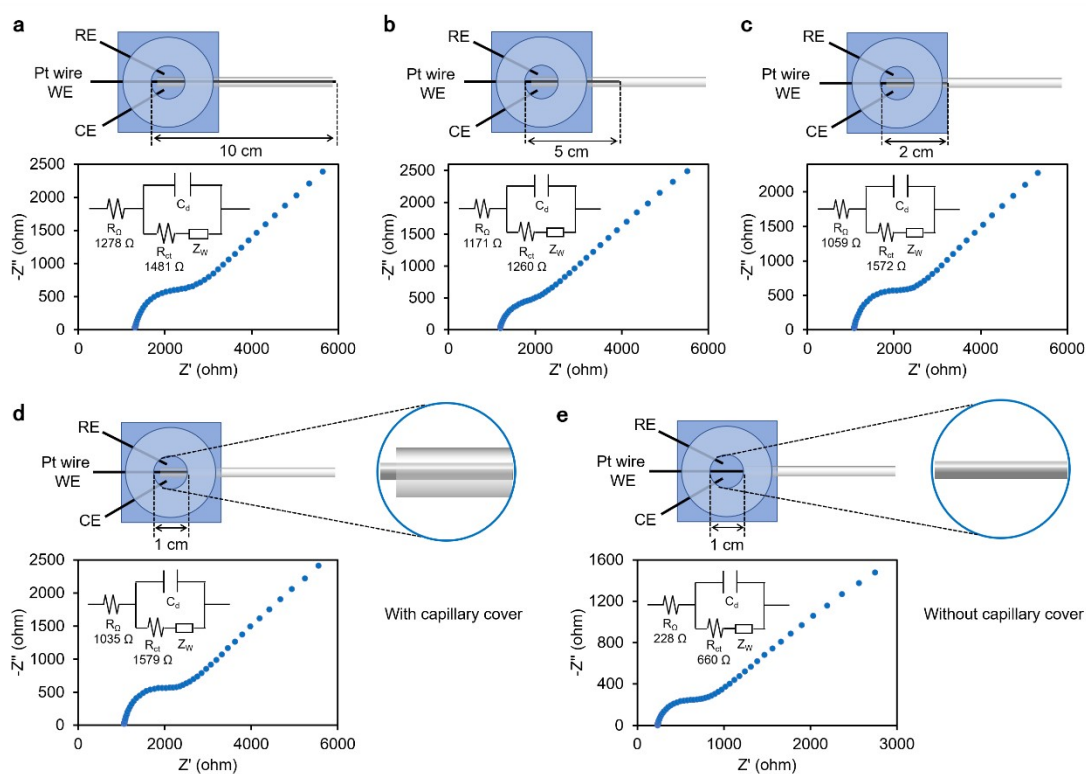


Figure S19. Schematics, electrical equivalent circuits and Nyquist plots of the electrochemical impedance spectroscopy of the RT-Triplex obtained in ACN/H₂O (1:1, v/v) containing 10 mM ammonium acetate and 1 mM K₃[Fe(CN)₆] and K₄[Fe(CN)₆] with varied exposure area of Pt wire WE. The extension length of Pt wire WE was adjusted to (a) 10, (b) 5, (c) 2 and (d, e) 1 cm. The difference between (d) and (e) is that the capillary part inside the reservoir was removed in configuration (e). The AC impedance measurements were carried out at an amplitude of 10 mV in the frequency range 100000-0.01 Hz.

The effect of electrolyte concentration on the impedance of the RT-Triplex platform was also evaluated. As shown in Figure S13, R_{Ω} and R_{ct} were determined to be 920Ω and 19846Ω , respectively, in ACN/H₂O (1:1, v/v) containing 10 mM ammonium acetate and 1 mM luminol. When the electrolyte concentration was increased to 100 mM, R_{Ω} decreased due to the enhanced conductivity of the solution, while R_{ct} did not change significantly. According to this experimental results, the increase in electrolyte concentration can improve the conductivity of the system, possibly conducive to the decrease of ohmic drop in the circuit. However, considering that electrolyte with concentration as high as 100 mM may suppress the ion signals of reactants, intermediates and products during MS detection, we eventually chose 10 mM ammonium acetate as the electrolyte, which is more compatible to MS.

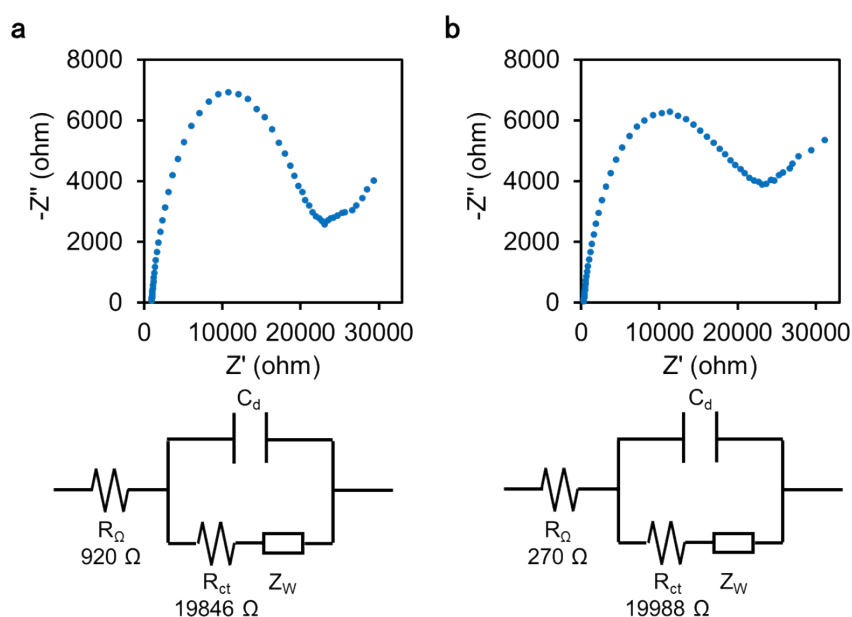


Figure S20. Nyquist plots of the electrochemical impedance spectroscopy and electrical equivalent circuits of the RT-Triplex obtained in ACN/H₂O (1:1, v/v) containing 1 mM luminol and the electrolyte of (a) 10 mM or (b) 100 mM ammonium acetate. The AC impedance measurements were carried out at an amplitude of 10 mV in the frequency range 100000-0.01 Hz.

Zoomed-in mass spectra of BODIPY⁺⁺ and by-products

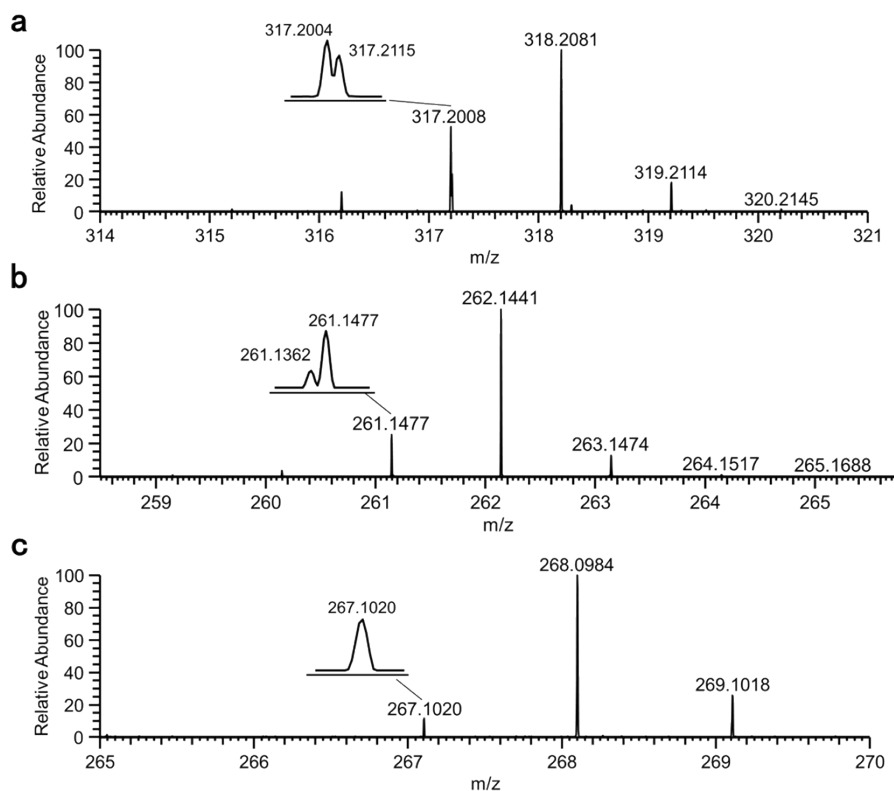


Figure S21. Zoomed-in mass spectra of (a) **B1a** (m/z 318.2081), **B1b** (m/z 317.2004), (b) **B2a** (m/z 262.1441), **B2b** (m/z 261.1362), and (c) **B3a** (m/z 268.0984) in positive ion mode upon applying to the WE the corresponding voltages (1.5 V for **B1** and **B2**, 3.0 V for **B3**).

Structural identification of the dehydrogenated by-products in the BODIPY system

Since the mass difference between BODIPY radical cation **B1a** and the by-product **B1b** (also for **B2a** and **B2b**) accurately refers to a hydrogen atom, we suppose the dehydrogenation might occur at the alkyl substituents. As a control, BODIPY **B3** with only one phenyl substituent shows only the corresponding radicals at m/z 268.0984 and no by-product supposed to be around m/z 267.0906 (Figure S19c and S20), further verifying the above speculation.

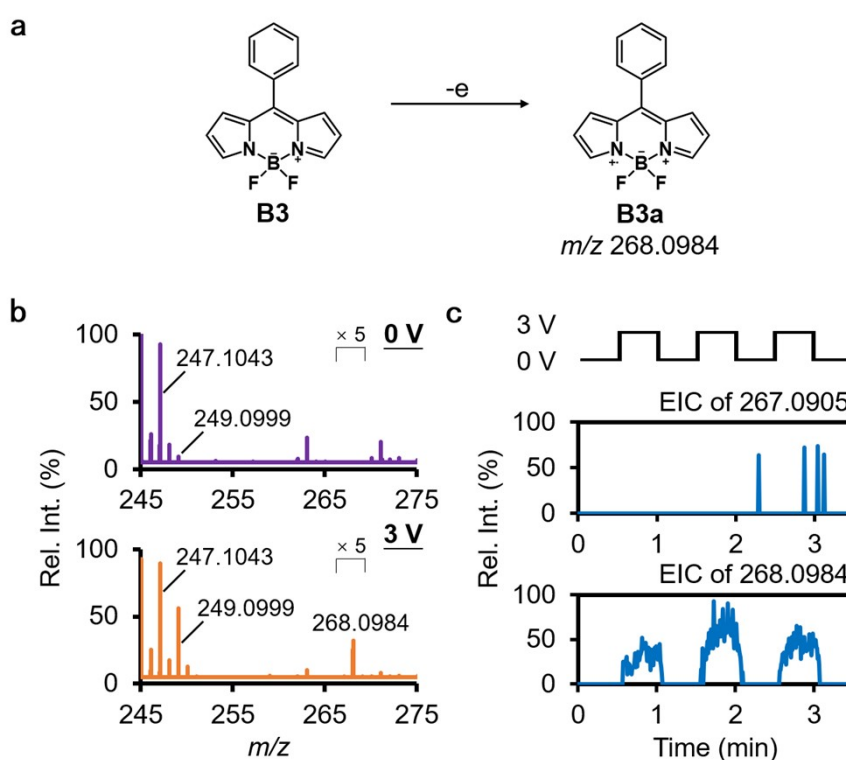


Figure S22. (a) Proposed mechanism for electrochemical oxidation of **B3**. (b) Positive-ion-mode mass spectra of 500 μM **B3** with 0 V and 3 V applied to the Pt wire WE. (c) The applied potential and EICs of m/z 267.0905 and m/z 268.0984 as the potential was switched between 0 V (30 s) and 3 V (30 s).

MS monitoring of dimerized BODIPY **B2** during electrooxidation

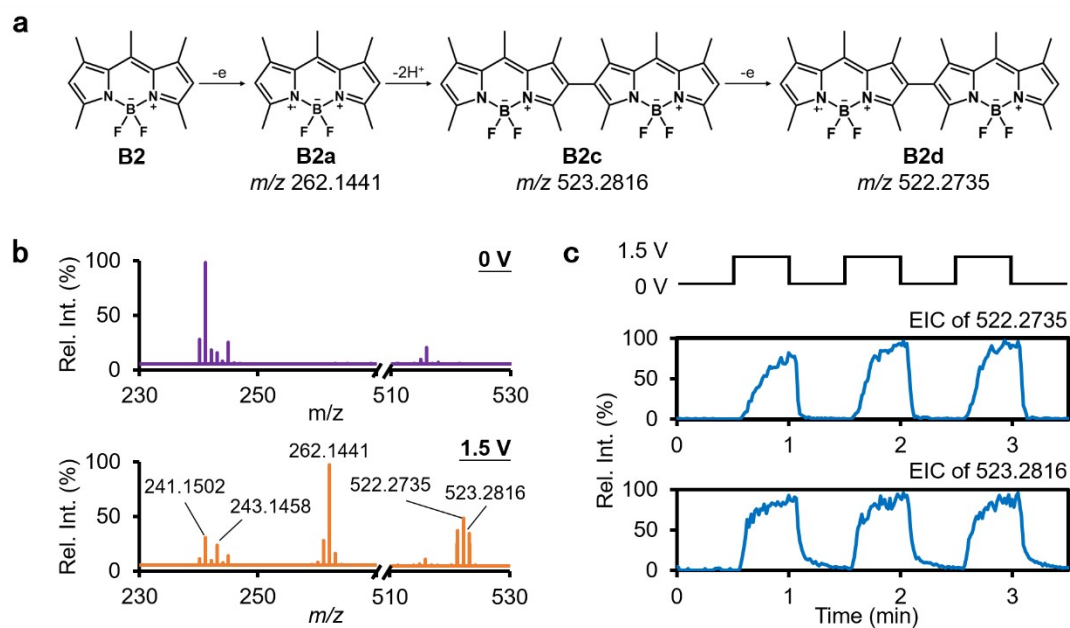


Figure S23. (a) Proposed mechanism for dimerization of **B2**.⁵ (b) Positive-ion-mode mass spectra of 250 μM **B2** with 0 V and 1.5 V applied to the Pt wire WE. (c) The applied potential and EICs of m/z 522.2735 and 523.2816 as the potential was switched between 0 V and 1.5 V.

MS/MS spectra of BODIPY⁺ and by-products

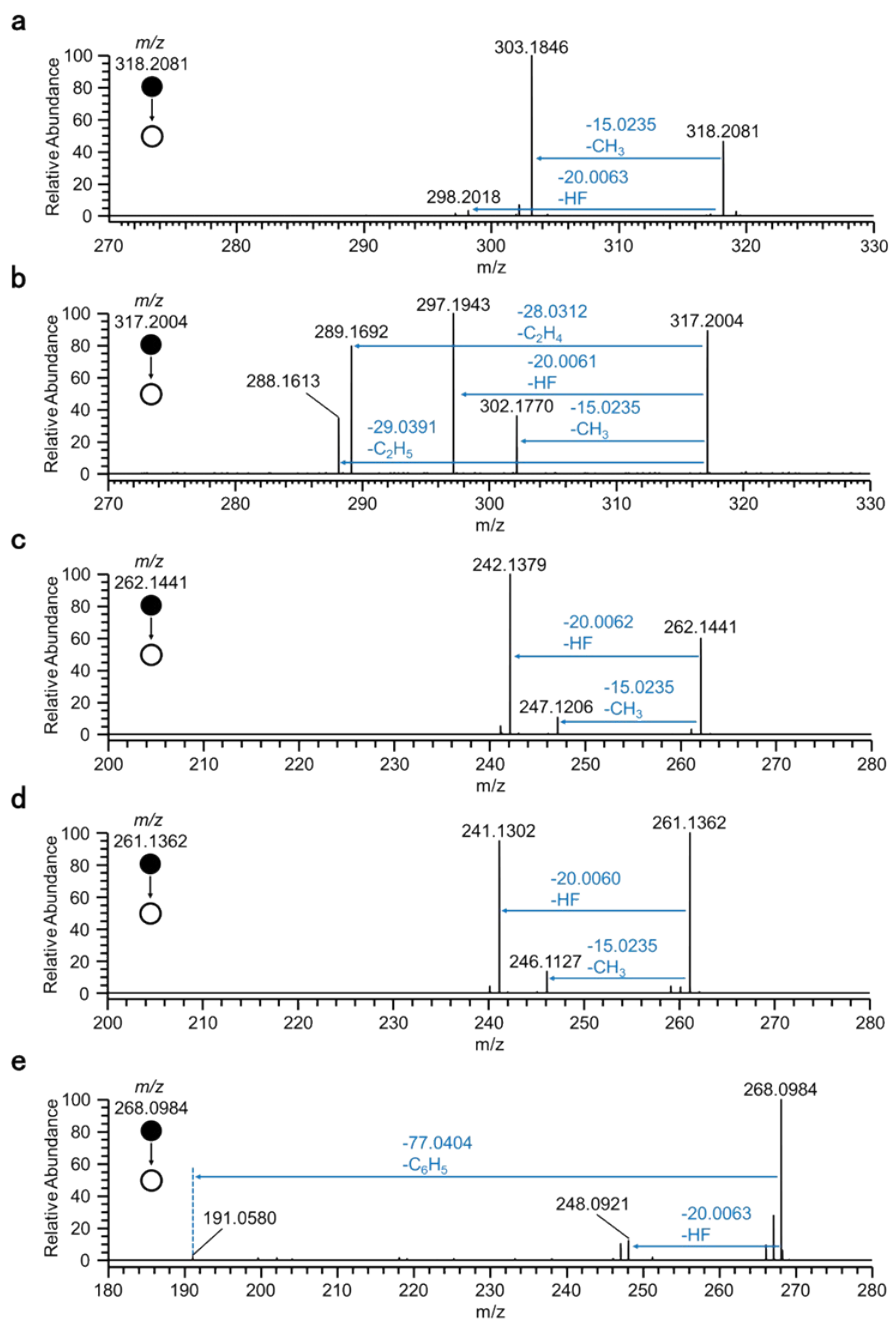


Figure S24. MS/MS spectra of (a) **B1a**, (b) **B1b**, (c) **B2a**, (d) **B2b**, and (e) **B3a** from the electrooxidation of BODIPY **B1**, **B2**, and **B3**.

The effect of increasing TPrA on electrogenerated species of BODIPY B1 and B2

To figure out which electrogenerated species in the BODIPY system reacted with TPrA, the ion signals of BODIPY^{•+} and [Pr₂N=CHET]⁺ were monitored by RT-Triplex while gradually elevating the TPrA level. The reservoir was first filled with 600 μ L ACN containing 250 μ M BODIPY, 2.5 μ M TPrA and 1 mM LiOTf, and then 10 μ L ACN solution of 0.1 mM TPrA was added into this electrolyte every two potential pulses during MS measurement. The N₂ pressure in VESI was fixed at 0.35 MPa to stabilize the flow rate of electrolyte at around 60 μ L/min. As shown in Figure S23, compared with the relative constant intensity of [Pr₂N=CHET]⁺, the BODIPY^{•+} signal dropped sharply as the concentration of TPrA increased in **B1** system. Similar responses of BODIPY^{•+}, dimer, and oxidized dimer were also observed in the case of the **B2** system (Figure S24).

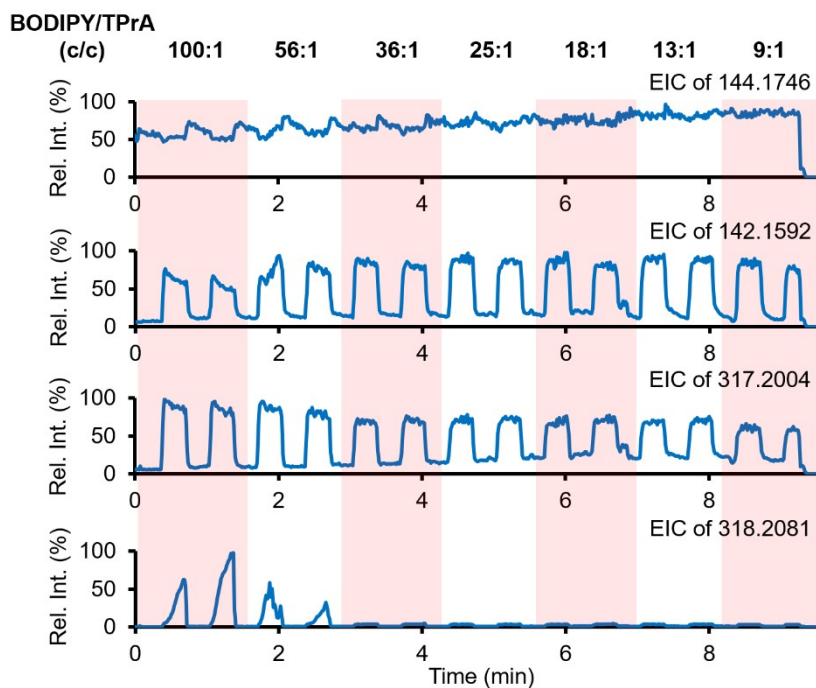


Figure S25. The EICs of m/z 144.1746, 142.1592, 317.2004, and 318.2081 in the BODIPY **B1** system as the concentration of TPrA gradually increases during repeated potential pulses. Potential pulses were given at 1.5 V with a duration of 20 s and an interval of 20 s.

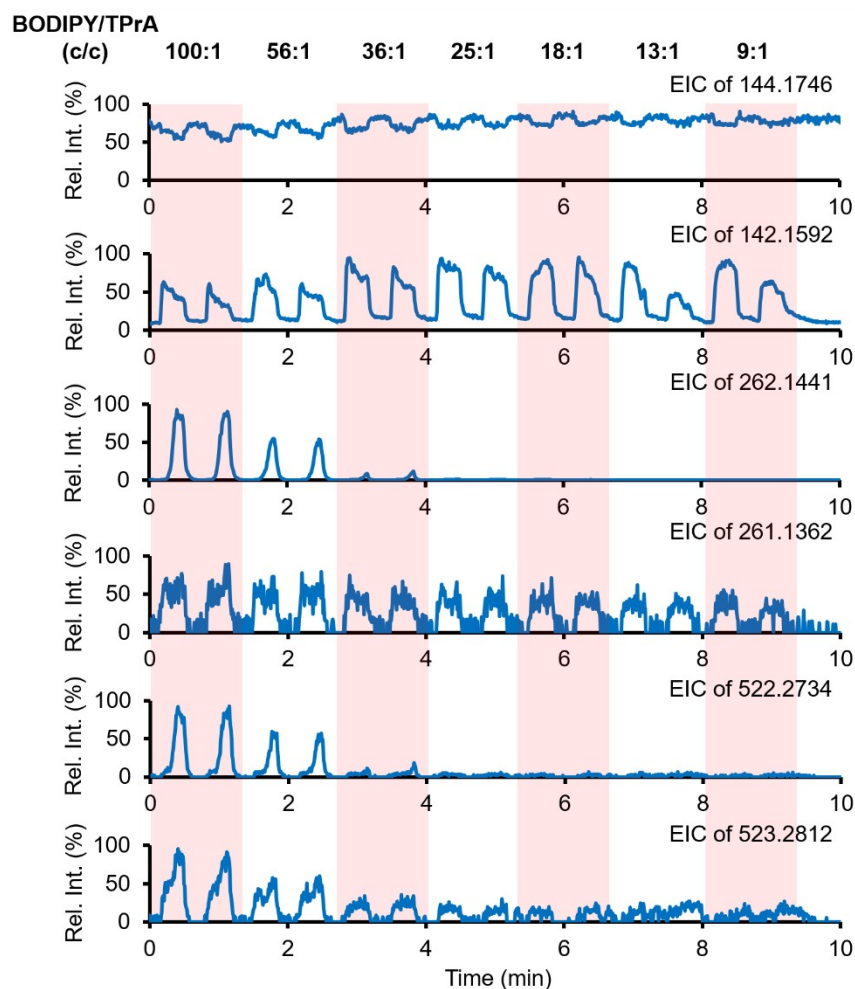


Figure S26. The EICs of m/z 144.1746, 142.1592, 262.1441, 261.1362, 522.2734, and 523.2812 in the BODIPY **B2** system as the concentration of TPrA gradually increases during repeated potential pulses. Potential pulses were given at 1.5 V with a duration of 20 s and an interval of 20 s.

Verification of the “catalytic route” in the BODIPY/TPrA ECL system

To verify that the ion $[\text{Pr}_2\text{N}=\text{CHet}]^+$ and ECL emission resulted from the homogeneous reaction between TPrA and BODIPY^{•+} formed in pre-anodization, we monitored TPrA injected post-anodization in the BODIPY-free system by RT-Triplex. Infusion of TPrA in the BODIPY-free electrolyte only resulted in the protonated ion signal of TPrA (m/z 144.1746) when no voltage was applied (Figure S25a-S25c). Even in the case that 1.5 V potential was applied on the WE for pre-anodization before the injection of TPrA, no signal from ECL or $[\text{Pr}_2\text{N}=\text{CHet}]^+$ was observed in the BODIPY-free solution (Figure S25d-S25f), proving that pre-oxidation of BODIPY must be the essential factor for the transformation of TPrA to $[\text{Pr}_2\text{N}=\text{CHet}]^+$.

Furthermore, a control experiment was performed by introducing the same volume (10 μL) of blank solution into the BODIPY **B1** system while tracking the ECL around the injection point. The ECL-time curve showed that rapid infusion of blank solution exerted no perturbation to the ECL output (Figure S26). In this sense, the flash of luminescence captured in Figure 6f should be attributed to the actual ECL emission from BODIPY^{*}.

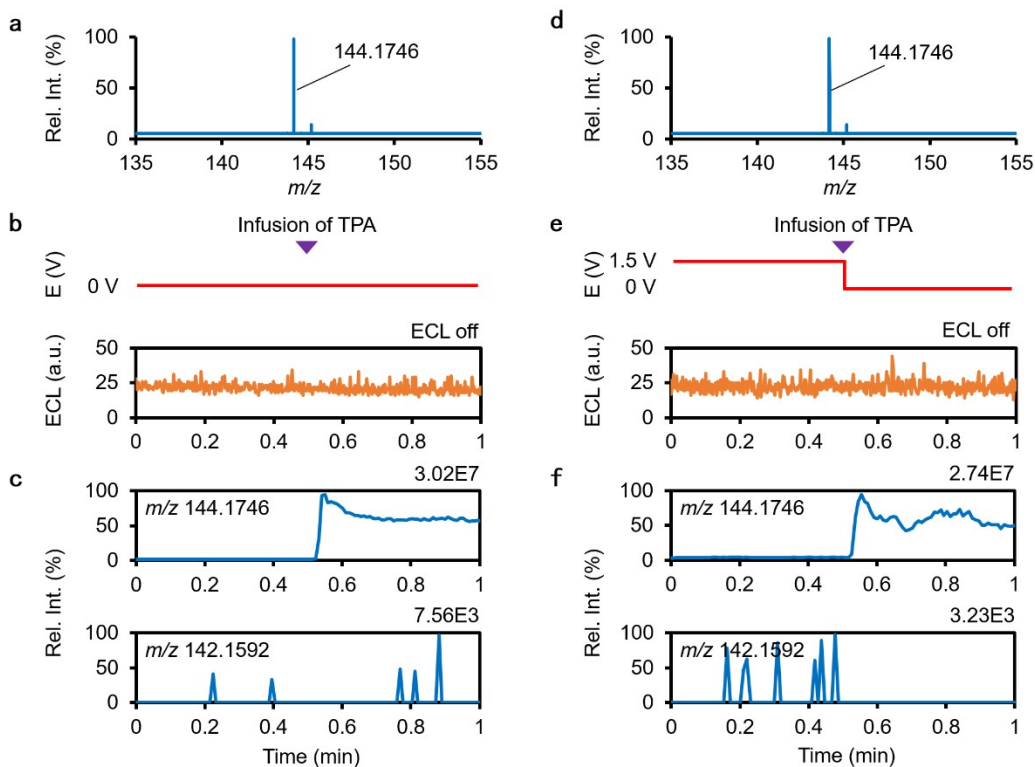


Figure S27. (a, d) Positive-ion-mode mass spectra, (b, e) applied potential, ECL-time curve, and (c, f) EICs of m/z 144.1746 and 142.1592 after infusion of 10 μL 1 mM TPrA into the blank solution (ACN containing 1 mM LiOTf) (a-c) without potential applied or (d-f) after switching the WE potential from 1.5 V to 0 V.

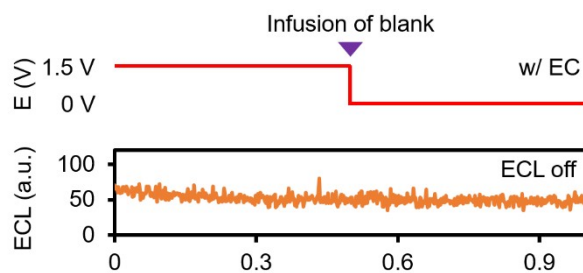


Figure S28. The applied potential and ECL-time curve before and after infusion of 10 μL blank solution (ACN containing 1 mM LiOTf) into the BODIPY **B1** system. The 1.5 V potential was applied on the WE for the beginning 0.5 min and switched off just before injection of the blank solution.

Cyclic voltammograms of TPrA and BODIPY B1

The CV curves of TPrA and **B1** in ACN containing 1 mM LiOTf were respectively recorded from 0 V to 1.5 V at scan rate 100 mV/s with a Pt wire as WE, a Pt wire as CE, and Ag/AgCl as RE. On the positive-going scan, a well-defined anodic peak at 1.07 V was observed for the electrooxidation of TPrA, while the oxidative peak potential of BODIPY **B1** was located at around 1.31 V. This observation indicates the redox potential of the BODIPY^{•+}/BODIPY couple is higher than that of TPrA^{•+}/TPrA, thus raising the possibility that TPrA could be oxidized to TPrA^{•+} by newly formed BODIPY^{•+}.

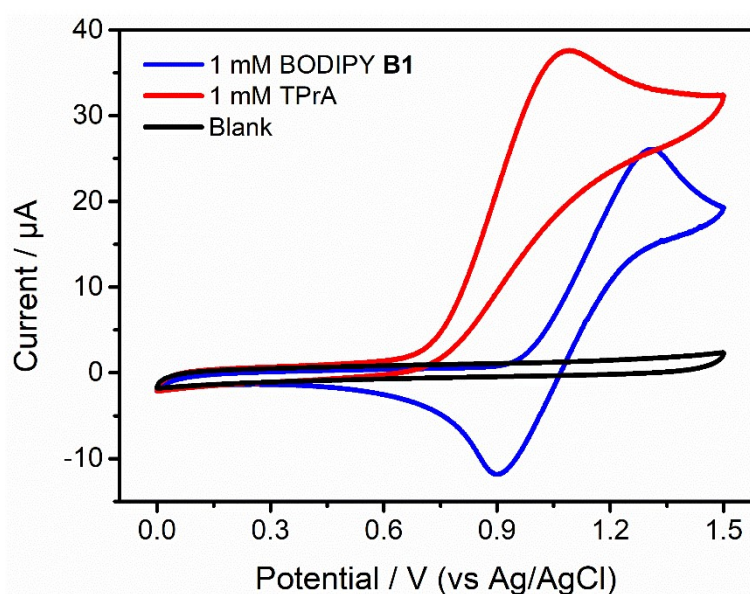


Figure S29. Cyclic voltammograms of blank solution, 1 mM TPrA, and 1 mM BODIPY **B1** in ACN containing 1 mM LiOTf on a Pt wire WE whose potential is varied from 0 V to 1.5 V at a scan rate of 100 mV/s.

Cyclic voltammograms of DMA, flunitrazepam, luminol and BODIPY in given conditions

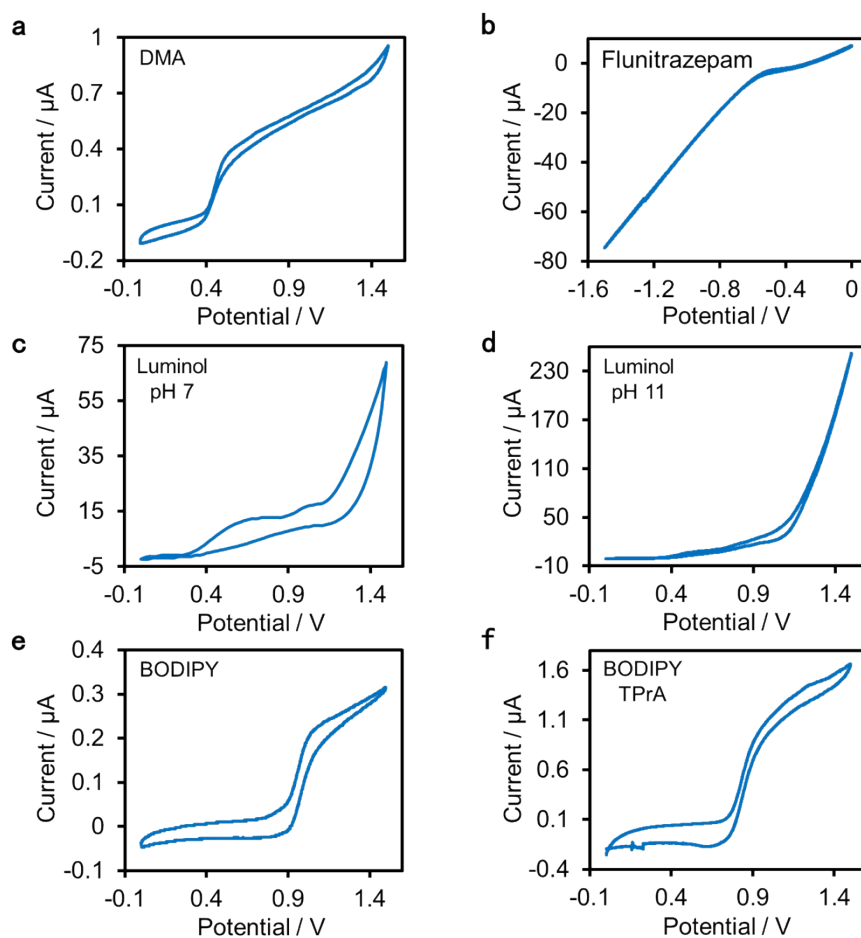


Figure S30. Cyclic voltammograms of (a) DMA, (b) flunitrazepam, luminol at (c) pH 7 and (d) pH 11, (e) BODIPY **B1** and (f) the mixed solution of BODIPY **B1** and TPrA rearranged from the data in Figure S4d, 2f, 3g and 4h in given conditions, respectively.

Table S1. Detailed information on intermediates and products from electrooxidation of DMA.

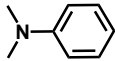
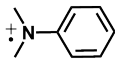
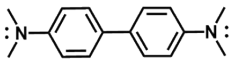
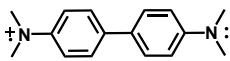
Analyte	Chemical structure	Chemical formula	Ion type	Theoretical m/z	Observed m/z	Relative error (ppm)
DMA		C ₈ H ₁₁ N	[M+H] ⁺	122.0964	122.0964	0
DMA ^{•+}		C ₈ H ₁₁ N ^{•+}	M ^{•+}	121.0886	121.0886	0
TMB		C ₁₆ H ₂₀ N ₂	[M+H] ⁺	241.1699	241.1699	0
TMB ^{•+}		C ₁₆ H ₂₀ N ₂ ^{•+}	M ^{•+}	240.1621	240.1621	0

Table S2. Detailed information on intermediates and products from electroreduction of flunitrazepam.

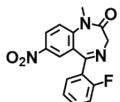
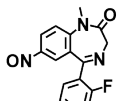
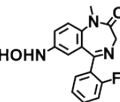
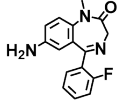
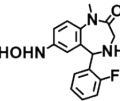
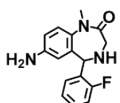
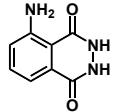
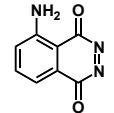
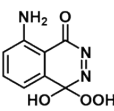
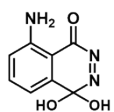
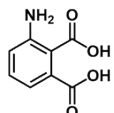
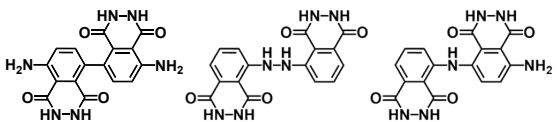
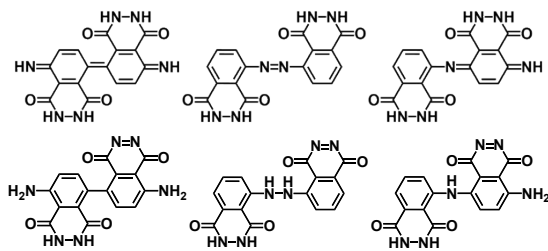
Analyte	Chemical structure	Chemical formula	Ion type	Theoretical m/z	Observed m/z	Relative error (ppm)
F1		C ₁₆ H ₁₂ FN ₃ O ₃	[M+H] ⁺	314.0935	314.0935	0
F2		C ₁₆ H ₁₂ FN ₃ O ₂	[M+H] ⁺	298.0986	298.0985	-0.34
F3		C ₁₆ H ₁₄ FN ₃ O ₂	[M+H] ⁺	300.1143	300.1141	-0.67
F4		C ₁₆ H ₁₄ FN ₃ O	[M+H] ⁺	284.1194	284.1192	-0.70
F5		C ₁₆ H ₁₆ FN ₃ O ₂	[M+H] ⁺	302.1299	302.1295	-1.32
F6		C ₁₆ H ₁₆ FN ₃ O	[M+H] ⁺	286.1350	286.1348	-0.70

Table S3. Detailed information on intermediates and products from ECL reaction of luminol.

Analyte	Chemical structure	Chemical formula	Ion type	Theoretical m/z	Observed m/z	Relative error (ppm)
Luminol (LU)		$C_8H_7N_3O_2$	$[M-H]^-$	176.0466	176.0469	1.70
Diazaquinone (L)		$C_8H_5N_3O_2$	$[M-H]^-$	174.0309	174.0308	-0.57
α -Hydroxy hydroperoxide (LHOOH)		$C_8H_7N_3O_4$	$[M-H]^-$ $[M-H-H_2O]^-$	208.0364 190.0258	208.0358 190.0255	-2.88 -1.57
LHOH		$C_8H_7N_3O_3$	$[M-H]^-$	192.0415	192.0412	-1.56
3-Aminophthalate (AP)		$C_8H_7NO_4$	$[M-H-H_2O]^-$	162.0197	162.0195	-1.23
Dimer		$C_{16}H_{12}N_6O_4$	$[M-H]^-$	351.0847	351.0847	0

Oxidized dimer

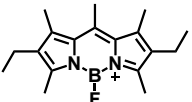
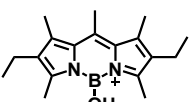
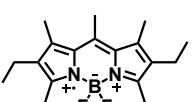
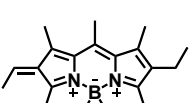
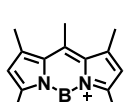
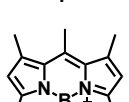
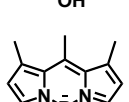
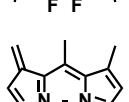
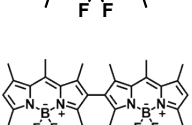
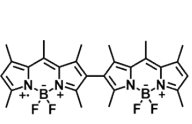
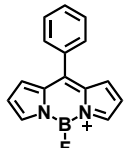


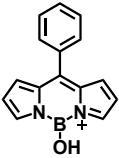
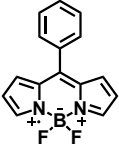
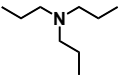
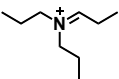
[M+H]⁺ 353.0993 353.0991 -0.56

[M-H]⁻ 349.0691 349.0689 -0.57

[M+H]⁺ 351.0836 351.0835 -0.28

Table S4. Detailed information on intermediates and products from ECL reaction of BODIPY.

Analyte	Chemical structure	Chemical formula	Ion type	Theoretical m/z	Observed m/z	Relative error (ppm)
B1-F		$C_{18}H_{25}BFN_2^+$	M^+	299.2089	299.2096	2.34
B1-OH		$C_{18}H_{26}BN_2O^+$	M^+	297.2133	297.2139	2.02
B1a		$C_{18}H_{24}BF_2N_2^{++}$	M^{++}	318.2073	318.2081	2.51
B1b		$C_{18}H_{25}BF_2N_2^+$	M^+	317.1995	317.2004	2.83
B2-F		$C_{14}H_{17}BFN_2^+$	M^+	243.1463	243.1458	-2.06
B2-OH		$C_{14}H_{18}BN_2O^+$	M^+	241.1507	241.1502	-2.07
B2a		$C_{14}H_{17}BF_2N_2^{++}$	M^{++}	262.1447	262.1441	-2.29
B2b		$C_{14}H_{16}BF_2N_2^+$	M^+	261.1369	261.1362	-2.68
B2c		$C_{28}H_{32}B_2F_4N_4$	$[M+H]^+$	523.2822	523.2816	-1.15
B2d		$C_{14}H_{16}BF_2N_2^{++}$	M^{++}	522.2744	522.2735	-1.72
B3-F		$C_{15}H_{11}BFN_2^+$	M^+	249.0994	249.0999	2.01

B3-OH		$C_{15}H_{12}BN_2O^+$	M^+	247.1037	247.1043	2.43
B3a		$C_{15}H_{11}BF_2N_2^{++}$	M^{++}	268.0978	268.0984	2.24
TPrA		$C_9H_{21}N$	$[M+H]^+$	144.1747	144.1746	-0.69
$[Pr_2N=CHEt]^+$		$C_9H_{20}N^+$	M^+	142.1590	142.1592	1.41

References

1. F. Tseliou, P. Pappas, K. Spyrou, J. Hrbac and M. I. Prodromidis, *Biosens. Bioelectron.*, 2019, **132**, 136-142.
2. K. C. Honeychurch and J. P. Hart, *J. Solid State Electrochem.*, 2008, **12**, 1317-1324.
3. J. N'Diaye and K. Lian, *J. Electroanal. Chem.*, 2019, **839**, 90-95.
4. V. Ferreira, A. C. Cascalheira and L. M. Abrantes, *Electrochim. Acta*, 2008, **53**, 3803-3811.
5. A. B. Nepomnyashchii, M. Broring, J. Ahrens and A. J. Bard, *J. Am. Chem. Soc.*, 2011, **133**, 19498-19504.